De Silva, G., Burgess, S., Hatano, T., Khan, S., Zhang, K., Nguyen Tien, T., ... Miles, M. (2016). An optimized nano-positioning stage for Bristol's Transverse Dynamic Force Microscope. In 7th IFAC Symposium on Mechatronic Systems & 15th Mechatronics Forum International Conference: Loughborough, United Kingdom, 5-8 September 2016 (pp. 120-126). (IFAC PapersOnline). Amsterdam:Elsevier. DOI: 10.1016/j.ifacol.2016.10.524

Peer reviewed version

Link to published version (if available):
10.1016/j.ifacol.2016.10.524

Link to publication record in Explore Bristol Research
PDF-document

University of Bristol - Explore Bristol Research
General rights

An optimized nano-positioning stage for Bristol's Transverse Dynamic Force Microscope

G. De Silva*, S.C. Burgess*, T. Hatano*, S.G. Khan*, K. Zhang*, T. Nguyen***, G. Herrmann*, C. Edwards***, and M. Miles**

*Department of Mechanical Engineering, University of Bristol, University Walk, Bristol, BS8 1TR, UK;
{G.Herrmann@bris.ac.uk}
**Centre for Nanoscience and Quantum Information, University of Bristol, Tyndall Avenue, Bristol, BS8 1FD, UK
***College of Engineering, Mathematics and Physical Sciences, University of Exeter, EX4 4QF, UK.
{C.Edwards@exeter.ac.uk}

Abstract: This paper presents the design process for the optimisation of a nano-precision actuation stage for a Transverse Dynamic Force Microscope (TDFM). A TDFM is an advanced type of Atomic Force microscope (AFM) that does not contact the specimen and therefore has potential for increased accuracy and decreased damage to the specimen. The nano-precision stage actuates in a horizontal plane within a region of 1µm×1µm and with a resolution of 0.3 nm. The non-contact TDFM has been developed at Bristol University for the precise topographical mapping of biological and non-biological specimens in ambient conditions. The design objective was to maximise positional accuracy during high speed actuation. This is achieved by minimising vibrations and distortion of the stage during actuation. Optimal performance was achieved through maximising out-of-plane stiffness through shape and material selection, as well optimisation of the anchoring system. The design was subject to constraints including an in-plane stiffness constraint, space constraints and design features relating to the laser interferometry position sensing system and subsequent controller design.

Keywords: x-y Stage, Force Microscope, Micro-/Nanosystems, Multi-Disciplinary Modelling, Motion Control

1. INTRODUCTION

Since its invention (Binnig et al. 1986), atomic force microscopes (AFMs) have become one of the most important tools to measure the 3-D topography of biological and non-biological specimens at a nano-scale (Hansma et al., 1986; Howland et al., 1993; Xu et al. 2010). The basic principle of an AFM is that a small cantilever mechanically scans the specimen in a raster fashion. The resolution of AFMs can be below 1 nanometre (1 x 10^{-9}m) enabling measurements of nano-scale specimens such as DNA and proteins (Garcia et al. 2007). A key advantage of AFMs is that they allow the observation of samples without changing their state or surroundings which is not the case with an electron microscope. Thus, this makes AFMs an ideal candidate for biomedical analysis in cancer research (Lekka et al. 2009), cell biology research (Hoh et al. 1992) and material science (Burnham et al., 1989).

Design optimisation of atomic force microscopes is important to achieve maximum resolution and speed of scanning. This paper deals with the optimisation of the horizontal x-y positioning stage of a particular type of force microscope, called a transverse dynamic atomic force microscope (TDFM). A TDFM is an advanced type of Atomic Force microscope (AFM) that does not contact the specimen and therefore has the potential for increased accuracy and decreased damage to the specimen.

1.1 Introduction to Bristol's Transverse Dynamic Force Microscope

A TDFM uses a vertically oriented cantilever (VOC) rather than a horizontal cantilever as the basic method for detecting a surface (TDFM) (Antognozzi et al. 2001; Brunner et al. 1999; Fletcher 2013; Harniman et al. 2012; James 2001). The basic layout of the TDFM at Bristol is shown in Fig. 1.
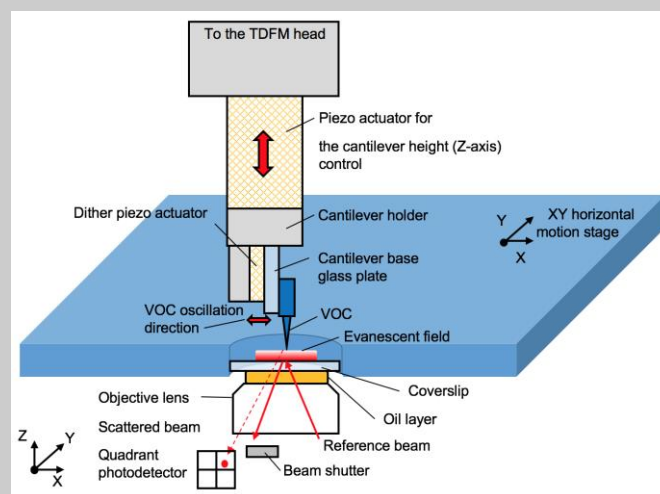

Fig. 1 : Basic positioning stage layout of TDFM

The specimen to be examined is placed on a nano-positioning stage that can be moved in a horizontal x-y plane. The vertical

cantilever is horizontally vibrated at a set frequency and placed above the specimen, but in close proximity, such that there is interaction with molecules of water within a microscopic water layer that covers the specimen. In ambient conditions, a specimen is usually covered with a thin water layer due to general humidity at room temperature and pressure (21°C, 100kPa). In particular, the first part of the layer, with a thickness of ~5nm, has well-ordered lattice-like structures of water molecules. The interaction with the water molecules results in the cantilever vibration being damped and the amplitude of vibration being decreased. The change in vibration of the probe is measured by a laser optical detection system, which is set beneath the thin quartz plate underneath the specimen (Antognozzi et al., 2008). Thus, when the specimen is moved in the x-y plane, the specimen topography can be measured by the probe at any particular position by keeping the vibration amplitude of the cantilever constant.

At present, the TDFM has a disadvantage in that the scanning speed is very slow. There is a need for the TDFM to scan faster so that they can monitor biological processes in real time. However, this requires a significant increase in scanning speed and this in turn requires a high accuracy of the nano-precision stage. The speed and accuracy of the TDFM scans are vitally dependent on the accuracy of the x-y positioning system holding the quartz coverslip with the specimen on top. Up to this point in time, the Bristol TDFM has used the high precision stage of Physik Instrumente, P-733.2, (Physik Instrumente, 2015a). This has a nominal resonance of 500 Hz which limited the bandwidth of any motion to less than 300 Hz. Other commercial precision stages for this purpose have, at best, resonance frequencies at about 2000 Hz (without load) (Physik Instrumente, 2015b). In order to obtain higher scanning speeds, a bespoke scanning stage is needed for the TDFM with a natural frequency well above 2000 Hz.

Hence, this paper considers the design and the subsequent control of a high precision stage. Section 2 discusses the basic set-up of the chosen positioning stage design. Section 3 introduces basic design concepts and Section 4 describes the first prototype, while Section 5 discusses the rigorous iterative design of the second prototype. Section 6 presents the practical results for the dynamics and control of the stage.
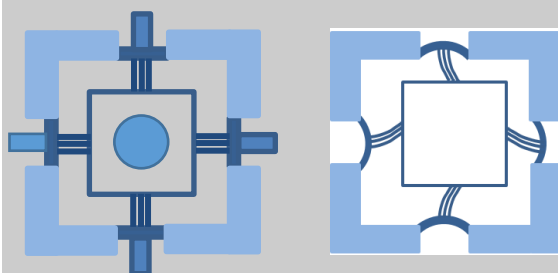
a)   b)
Fig. 2: Basic stage layout a) with actuator b) with bent/displaced beam structure

2 THE X-Y POSITIONING SYSTEM

The nano-positioning system consists of three main elements: a flexible structural element, actuators, and position sensors as shown in Fig. 2. The flexible structural element (see for instance Polit et al. (2009) for discussion on flexures) is capable of being moved in the x-y plane via two perpendicular actuator pairs. The simple schematic design of the beams is shown in Fig. 2 showing an un-displaced and displaced position of the beams. Piezoelectric (piezo-) actuators (P-885.11, Physik Instrumente. (2015c)) are used because of their high stiffness, linear displacement and high load capacity. The specimen is held on a glass slide in the centre of the structural element with a hole in the middle of the stage for the optical lens of the cantilever detection system. A laser-interferometer system (Zygo ZMI 2402 with laser head ZYGO ZMI 7702) is used to detect movement in the x-y plane, as it does not limit the bandwidth of the position detection system and it provides positioning accuracy of 0.3 nm. This symmetric layout is inspired by the stage produced by Schitter et al. (2006), as it permits equal performance in x- and y-positioning, which is for instance ideal for non-raster scanning. This also contrasts non-symmetric and more complex structures such as those suggested by Polit et al. (2009), Yao et al. (2007), Leang (2008) or Yong et al. (2009), which would not fit the requirements of the investigated TDFM.

2.1 Design constraints and objectives

The positioning system has the following constraints and requirements:
a) The design space for the structural element is 93 mm x 93 mm x 10mm;
b) the structural element must be able to displace up to 1 micron in the x and y axes;
c) the stage must possess a specimen holder consisting of a circular quartz plate of 16mm to 24mm diameter.

Out-of-plane vibrations decrease the accuracy of the relative placement of the cantilever in the Z-direction. Hence, this increases the demand on a Z-axis controller of the cantilever. Decreased accuracy of the 3D topography measurement of the specimen may result from such an out-of-plane motion.
Therefore, the overall design objectives for the nano-positioning stage are:
a) smallest natural frequency > 7 KHz;
b) minimal out-of-plane displacements < ~ -25 dB compared to the in-plane displacement

3. CONCEPTUAL DESIGN

3.1 Material selection

The best material for achieving high frequency is the one with the highest value of

$$\sqrt{E/\rho}, \quad (E= \text{Young's modulus, } \rho = \text{density})$$

There is an additional advantage in having a high Young's modulus E because a higher modulus allows thinner sections to be made. The reason for this is that the thickness of thin sections is limited by buckling performance and buckling performance is directly proportional to the material modulus.

The main candidates for the position stage are steel, aluminium and titanium. Table 1 shows steel ranked third behind titanium and aluminium for frequency. However, there is only around 8% difference between titanium and steel so the range of

performance for $\sqrt{E/\rho}$ is not that large. In terms of buckling performance, steel is ranked first by a large margin. Therefore, steel was chosen because of its ability to form thin sections whilst still achieving a comparable frequency performance to other materials. This is also confirmed by the fact that titanium and steel have similarly low thermal expansion coefficients, while Aluminium's is more than twofold the value of titanium and steel.

	E	ρ	$\sqrt{E/\rho}$	Thermal Coef-ficient α	Rank frequency	Rank modulus	Rank Thermal Expansion
	GPa	kg/m^3	m/s	$\mu m/\ (K{\cdot}m)$			
Steel	193	8080	4887	10.8	3	1	2
Aluminium	69	2710	5042	23.1	2	3	3
Titanium	114	4043	5310	8.1	1	2	1

Table 1: Material properties for selection of stage material (E=Young's modulus, ρ=density)

3.2 Overall stiffness and pre load selection

To maximise natural frequency, it is necessary to maximise in-plane stiffness. A push-pull layout is chosen because this gives more symmetry to the displacement. The push-pull layout selected requires 2 piezo actuators per axis. Compressive preloads between the actuators and the structure are necessary to avoid backlash. They sum across the push-pull set-up. Hence, to compute for each actuator its own preload, for the chosen actuator arrangement (two P-885.11 actuators for each direction) a blocking force of 400N needs to be considered. The maximum actuation voltage was ±60V and a maximum unrestricted displacement of 4 μm for the operating voltage of 60V (Fig. 3).
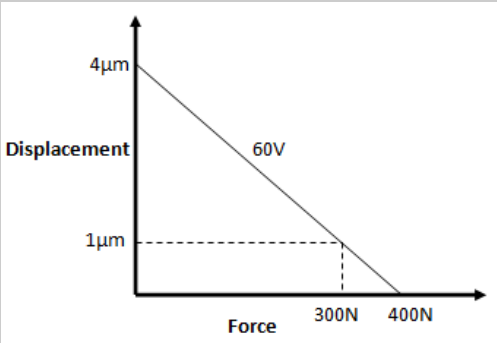

Fig. 3 : Piezo actuators force to displacement relationship at 60V

To displace 1 micron the maximum preload is 300N. Therefore the preload requirement per actuator is 300N to permit the actuator to displace the stage by 1 μm. This preload limits the actuation voltage to ±60V. Since a displacement of 1 μm is required in the x and y directions, this means that the optimum stiffness of the stage was 600N/μm. The piezo-actuators

stiffness is around 18% of the stage stiffness so they add a significant amount of extra stiffness.

4 PROTOTYPE 1: DESIGN AND PERFORMANCE

4.1 Design description and rationale

The first prototype positioning stage design is shown in Fig. 4. The rationale for the three beams holding the central specimen section is to give high torsional stiffness. The reason for the enclosed square for holding the specimen is to give stiffness to the central section. The base of this square has a plate to hold the specimen holder. There are two vertical mounts (flags), one on each axis, protruding from the edge of the specimen holder. They are used for the attachment of thin mirrors, acting as reflectors for the two laser beams of the laser interferometer. The 'T shaped' side clamps in this design are used to apply/adjust the mechanical preload applied to the piezo actuators.
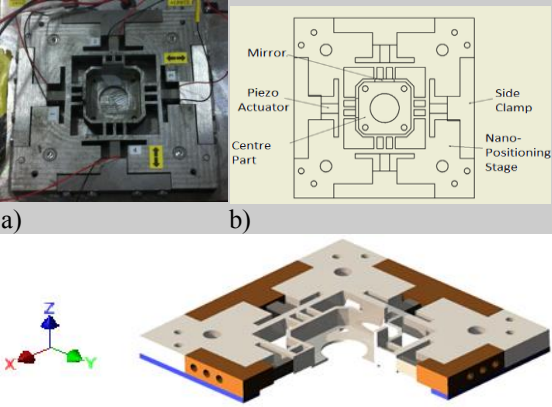

Fig. 4 : Bristol TDFM 1st high-speed-stage Prototype: a) 1st High Speed Stage Prototype; b) 1st High Speed Stage's Schematic; c) ¾ Section of the 1st High Speed Stage prototype showing z-axis asymetry with plate at bottom in the centre part

4.2 Testing of structural performance

Practical Swept Sine System Identification was carried out for the first prototype and its frequency responses have been obtained, identified with XX (excitation in the X-direction and translational X-direction measurement), XZ (excitation in the X-direction and translational Z-direction measurement), YY or YZ.
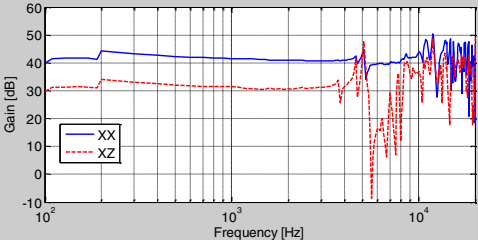

Fig. 5: Performance [nm/V] of the 1st high-speed-stage Prototype in the frequency domain using a high bandwidth piezo-amplifier with voltage gain of 15

Even though this stage performed with its first resonance frequency as high as ~7.8 kHz, Prototype 1 generated a

significant amount of out-of-plane vibrations in the transverse direction once actuated in-plane. Fig. 5 presents the amplifier input to translational output frequency Bode-plot derived from a swept sine analysis. It can be clearly seen that there is a difference between the in-plane and the out-of-plane motion of ~10dB at low frequency, which provides an equivalent relative gain factor of ~3.16 between the XX and XZ amplitude plot. This performance is much worse than acceptable. Note also the discontinuities in the amplitude plot in low frequency which are to be eradicated for the next prototype, Prototype 2. This prototype will have a completely flat bottom surface on the TDFM base and equally well-distributed clamping forces for avoidance of such dynamic effects.

The prototype 1 design was subjected to Finite Element Analysis (FEA) in order to gain further insight into its performance. During this FEA of prototype 1, all the piezo-actuators are perfectly aligned. Therefore, it can be concluded that the out-of-plane behaviour is solely due to its structural features. The specimen holder centre part has a plate at the bottom of the stage (see Fig. 4c). This introduces a lack of symmetry in prototype 1 in the z-direction which is the largest contributor to the out-of-plane behaviour. Therefore, it was concluded that the next prototype should be designed with vertical symmetry for minimum out-of-plane vibrations while improving/maintaining its speed of operation and also introducing symmetry in the other principal directions.

5. PROTOTYPE 2 DESIGN AND OPTIMISATION

5.1 Physically Idealised Model and Design Development

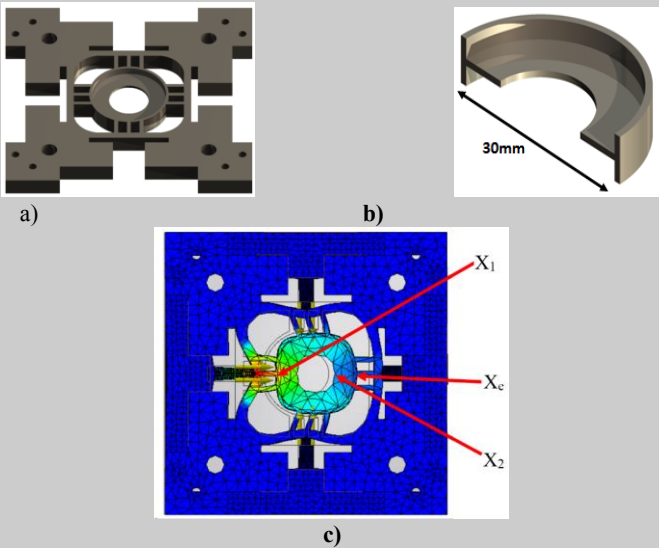a)   b)

c)

Fig. 6 : Physically idealised model with the new Centre Part: a) Physically Idealised Model; b) stage-centre-part with I beam cross section; c) FEA: Deformation difference vs loading

A new high-speed-stage structure is proposed and this is subjected to a continuous optimisation process upon application of geometric changes and tuning using Computer Aided Design (CAD) and FEA. Autodesk Inventor (Autodesk, 2016) was chosen for this task as it allows for structural changes and fast FEA results. A physically idealised model as shown in Fig. 6a is designed using the old high-speed-stage structure, where the old square shaped stage-centre-part is replaced with a circular Centre Part. The cross section of the new centre part has an 'I beam' cross section and this salient feature inherits a higher second moment of area than the old asymmetric square centre part, thereby inducing less structural bending upon actuation. As a basic requirement, the positioning stage symmetry across its XY plane is to be maintained and its in-plane stiffness is to be achieved at 600N/µm for any structural feature added/changed. Similar to the 1st high-speed-stage prototype, three beam flexures are applied at each side as this provides a greater torsional stiffness thereby minimizing coupling of X and Y motion. The physically-idealised model itself demonstrates superior performance over prototype 1 especially in terms of its resonance and out-of-plane displacements as shown in Table 2. The FEA of the physically-idealised-model is tested for its maximum piezo-actuator loading of 600N.

As the FEA assumes perfect symmetry of the physically idealised model/high-speed-stage, an out-of-plane displacement phenomenon is deliberately induced in the FEA, by deliberately misaligning the piezo-actuators. During this analysis, one piezo-actuator is moved up by 0.5mm while the other is moved down by 0.5mm. For all the FEA carried out, this misalignment is applied to artificially introduce and subsequently measure out-of-plane displacements.

Resonance (kHz)	8671
In-plane stiffness (N/µm)	517
Max out-of-plane displacements (µm)	0.453
% increase of resonance	10.4
% reduction of out-of-plane displacements	90.6

Table 2 - Properties of the physically-idealised-model

The physically-idealised-model was subjected to a series of structural changes in order to obtain its optimum performance in terms of resonance, out-of-plane displacements and accuracy of the scan measurements. The high-speed-stage was tuned to retain 600N/µm, and its resonance increased to 10 kHz.

During the FEA, it was discovered that the centre part of both the old and the new high-speed-stage deformed due to the piezo-actuator loading. It is a crucial requirement to reduce this undesirable centre-part deformation due to its impact on the overall measurement accuracy. During centre-part deformation, the specimen coverslip is prone to slide over the centre part surface. Therefore, the displacement of the specimen will not be the same as its demanded displacement. Hence, it is necessary to strengthen the structure of the stage-centre-part.

5.2 Analysis of Centre Specimen Stage Deformation

Fig. 6b shows the centre of the stage-centre-part. During the FEA it was found, that the stage-centre deforms differently to its edge. Thus, the phenomenon of a deformed middle-edge relationship of the stage-centre-part was further tested using FEA. The preloaded stage was actuated from 100-600N. The difference of deformation (X1-X2) of the stage-centre-part,

varies linearly with the piezo-actuator loading. For an effective force of 600N the difference in displacement is 1.2µm. This difference of displacement per force almost equals the required in-plane stiffness of 600N/µm, which is highly undesirable. Hence, it is necessary to strengthen this stage-centre-part so that the TDFM scanning accuracy is improved.

5.3 Shape Optimisation- Structural Strengthening of Stage-Centre

A parametric analysis was carried out in order to determine the features and the dimensions necessary for the high-speed-stage to give the most optimum results in terms of resonance and scanning accuracy. During this optimisation process, it was necessary to increase the structural stiffness of the stage-centre-part while trading off other features for this increase in stage-centre-part stiffness. The target was to achieve an overall plane stiffness of 600N/µm. The ideas proposed to reduce the observed deformation include: an increase of the base thickness, application of fillets/chamfers and corrugated profiles to the stage-centre-part.

5.3.1 Base Thickness Variations

The in-plane stiffness k of a structure as shown in Fig. 6 is directly proportional to its cross sectional area A in m^2, the elastic modulus of the material E in Pa, and is inversely proportional to the length of the structure l in m:

$$k = \frac{EA}{l}$$

During this analysis, the base thickness was increased, while keeping the diameter of the stage-centre-part constant.

5.3.2 Wall Chamfers and Fillets

Different sizes of chamfers and fillets were tested on the inner wall of the stage-centre-part. Chamfers prove superior to fillets in terms of improving the stage-centre-part stiffness. 45º chamfers were chosen over other chamfer/filler options, as this reduced the stage-centre-part deformation from 0.85 to 0.46µm. However, this again reduced the resonance by ~1kHz, which was considered an acceptable trade-off.

5.3.3 Shape - Optimising the Resonant Frequency

Another parametric analysis was carried out to push the resonance frequency higher using FEA, especially to compensate the resonance frequency reductions during the optimization of the stage-centre-part. The most suitable features to tune were identified as the piezo-actuator-flexure boundary, T, and the flexure gaps, G, W and L, as shown in Fig. 7a and Fig. 7b.
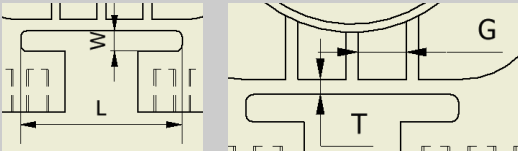
Fig. 7 - Identified features to tune the stiffness

Their dimensions were varied in a manual iterative process, whilst maintaining a constant in-plane stiffness of ~600N/µm.

5.4 Evaluation of the CAD Model

The performance of the new high-speed-stage (see Fig. 7 for centre part and Fig. 8 for the manufactured stage) as observed in a FEA is shown in Table 3.

Resonance (kHz)	In-plane stiffness (N/µm)	Max out-of-plane displacements (µm)	$X_1 - X_2$ (µm)
~7.14	595	0.38	0.358

Table 3: Performance of the new high-speed-stage

Considering the measurement point in Fig. 5c and the results from Section 5.2 in relation to Table 3, the measurement accuracy of the new high-speed-stage proved superior, because the relative change in displacement of the two measurements points X1 and X2 is now significantly reduced from 1.2µm for the idealized model in Section 5.2 to 0.358µm for the optimized stage. This is also much better than for the old high-speed-stage (the prototype 1). There the FEA analysis showed that the change in displacement was much worse at 4.68µm.
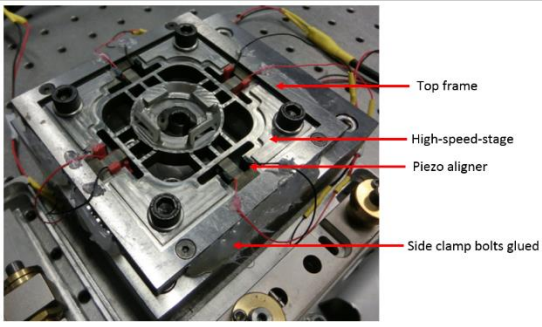

Fig. 8: - High-speed-stage (Prototype 2) after all the post manufacturing modifications
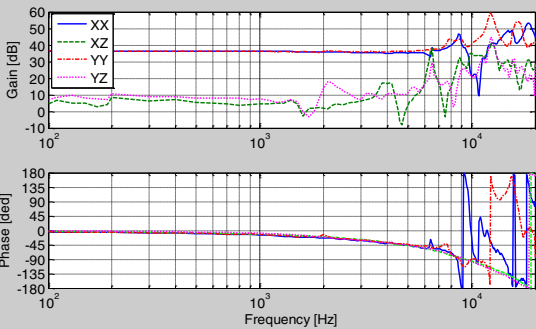
Fig. 9: Performance [nm/V] of the high-speed-stage (Prototype 2) upon post-manufacturing optimisation

6 PROTOTYPE 2 – DYNAMICS & CONTROL

6.1 Practical Dynamic Performance

The measured performance of the manufactured high-speed stage (Fig.8) is seen in the frequency plots of Fig. 9 with matching dynamics in both X and Y directions. These measurements also include the filter dynamics of the laser interferometer and the minor delay of the National Instrument data oscilloscope and data processing system, NI PXI-5122. The low frequency gains of both X to X and Y to Y motion are now identical at an increased value of ~-25dB [nm/V]. The gain difference for the out-of-plane displacements frequency responses in relation to their respective in-plane displacement

frequency behaviour have been set to a value of ~25dB at low frequency. The out-of-plane displacements gradually increase near 6 kHz. This frequency is identified as the high-speed-stage's first resonance after all the post manufacturing modifications. This frequency is around 1 kHz lower than the ~7.3 kHz observed during the FEA.

6.2 Controller Design

The overall implementation setup is briefly described prior to the controller design. Fig. 10 shows the high-speed-stage system configuration.
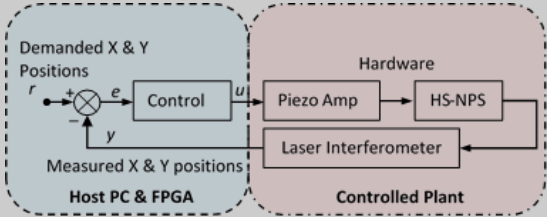

Fig. 10: Control loop structure

The high-speed-stage, the high-bandwidth piezo amplifier and the laser interferometer are treated as the controlled plant. The measured stage displacements in the X- and Y-axes are fed back to an FPGA based control implementation system from National Instruments (PXI-7854R), which can provide fast parallel computations and time-deterministic operation. The demanded stage positions, filters and the controllers were implemented on this FPGA board with a sample frequency of 100kHz. Based on the identified X and Y stage dynamics, the closed-loop controllers were designed in order to minimize the tracking errors, piezo nonlinearity, disturbances and the oscillatory behaviour due to the excitations of the stage resonances at ~6.5kHz and ~9kHz.
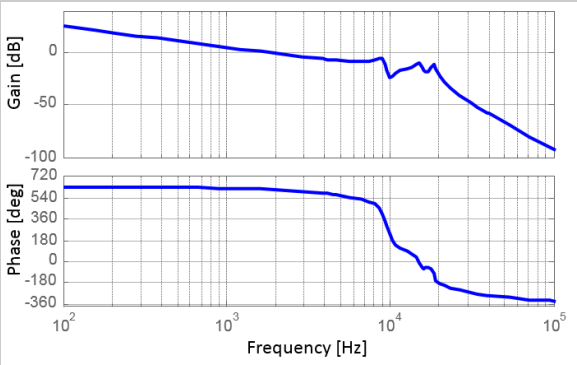
Fig. 11: Open-loop dynamics in the X-axis. Gain margin: 8.61dB at 5.83 kHz, Phase margin: 65.3deg at 1.73kHz.

The frequency-shaped controller is of 4th order so that it does not consume space on the FPGA. The gain and phase margins of this open-loop system are 8.61dB and 65.3degrees, respectively (Fig. 11). This guarantees a robust and stable closed-loop system.
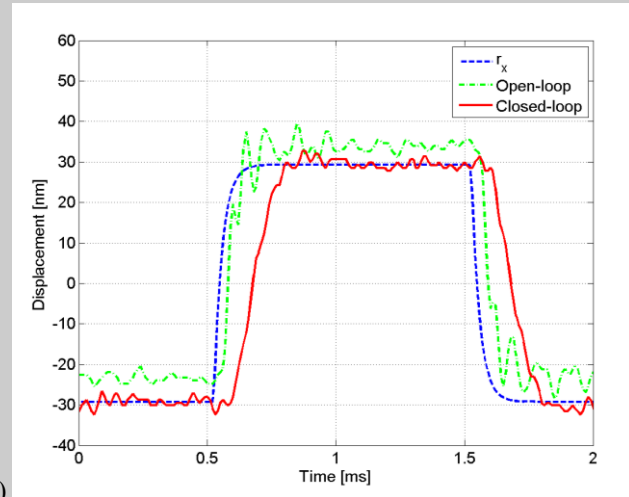
Note that the controller for the Y-axis was designed in a similar manner and so the corresponding bode plot is omitted for the sake of brevity.

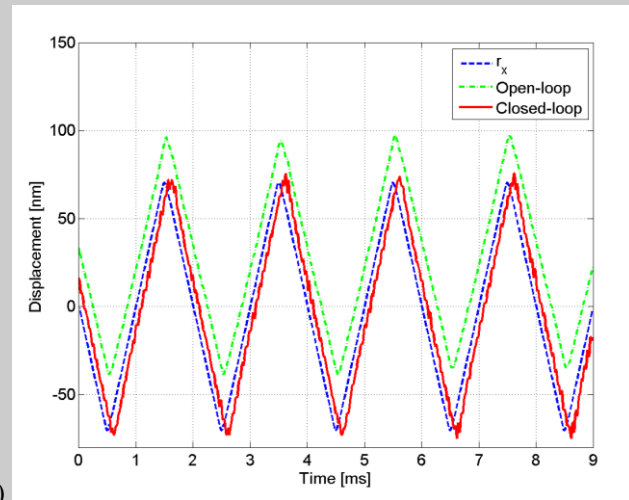## 6.3 Comparative Implementation Tests Results

To verify the performance of the designed controller, comparative benchmark tests (i.e. with and without the controller) were carried out.
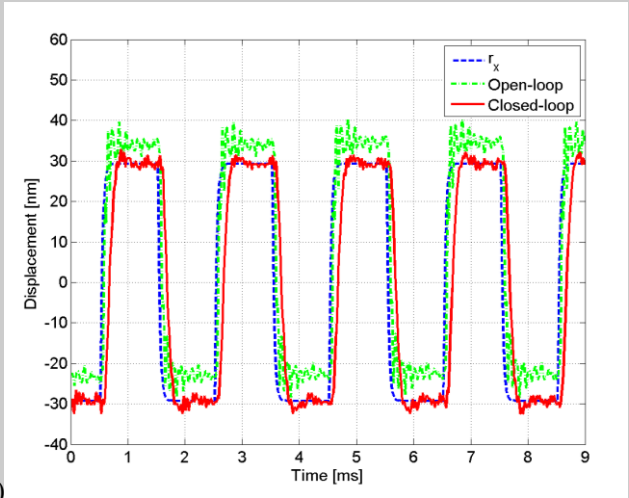
a)

b)

c)

Fig. 12: Positioning performance with and without control: (a)-(b) Square wave (b) Triangular wave tests.

As seen from Fig. 12a-b, large overshoots, steady-state errors and oscillatory responses were observed for the stage without

the controller. Furthermore, its response also drifts due to piezo hysteresis. This can cause a distorted scanned image.

On the other hand, with the controller, stable and accurate tracking was maintained without the drift issue. In addition, a settling time of ~0.4ms was achieved. Fig. 12c depicts the test results for a triangular wave demand at 500Hz. The open-loop controller does not work well due to the piezo drift, however the closed-loop strategy shows satisfactory demand signal following performance. This is also easily quantitatively documented. In the case of the triangular demand, the root-mean-square (RMS) error value with respect to the demand is 30nm while for the closed loop strategy it is 13nm.[1]

The stage resonances at ~6.5kHz and ~9kHz are successfully compensated for by the controller. In this case, a closed-loop bandwidth of ~2kHz has been obtained. Moreover, noticeable out-of-plane dynamics in the high-frequency region are also reduced. Thus, the high-speed-stage together with this controller can achieve precise high-speed scanning. Note that the Y-axis test data are omitted in this paper since the results in the Y-axis are similar to those of the X-axis due to the symmetric structure of the high-speed-stage.

7   CONCLUSIONS

A bespoke high-speed stage has been designed for the transverse dynamics force microscope (TDFM). This stage was specially designed for minimal cross-axis interaction and guarantees maximal symmetry in the x/y/z directions subject to design and system constraints. The design steps provide general guidance for increasing of resonance frequency while retaining stiffness, so that the applied piezo-actuators permit the required unstrained 1μm×1μm motion to be achieved. An overall resonance frequency of 6 kHz is achieved allowing a closed loop-control frequency of 1.73 kHz for precise horizontal motion control.

8   ACKNOWLEDGMENTS

References

Autodesk (2016) 3D CAD software for engineering design Accessed 9 Feb 2016, from website: http://www.autodesk.co.uk/products/inventor/overview.

Antognozzi, M., Ulcinas, A., Picco, L., Simpson, S. H., Heard, P. J., Szczelkun, M. D., Brenner, B. and Miles, M. J., 2008, "A new detection system for extremely small vertically mounted cantilevers," Nanotechnology, vol. 19, no. 38, p. 384002.

Antognozzi, M., Humphris, A., and Miles, M., 2001, "Observation of molecular layering in a confined water film and study of the layers viscoelastic properties," Applied Physics Letters, vol. 78, no. 3, pp. 300–302.

Binnig, G. Quate, C. and Gerber, C., 1986, "Atomic force microscope," *Physical Review Letters*.

Brunner, R., Marti, O., and Hollricher, O., 1999 , "Influence of environmental conditions on shearforce distance control in near-field optical microscopy," Journal of Applied Physics, vol. 86, pp. 7100–7106.

Burnham, N. A. and Colton, R. J., 1989, "Measuring the nanomechanical properties and surface forces of materials using an atomic force microscope," Journal of Vacuum Science Technology.

Fletcher, JM, Harniman, RL, Barnes, FRH, Boyle, AL, Collins, AM, Mantell, J, Sharp, TH, Antognozzi, M, Booth, PJ, Linden, N, Miles, MJ, Sessions, RB, Verkade, P & Woolfson, DN 2013, 'Self-assembling cages from coiled-coil peptide modules' Science, vol 340, no. 6132, pp. 595-599.

García, R., Magerle, R., & Perez, R. (2007). Nanoscale compositional mapping with gentle forces. Nature materials, 6(6), 405-411.

Hansma P.K., Schitter G., Fantner G.E. & Prater C. (2006). High-Speed Atomic Force Microscopy. Science, 314.

Harniman, R. L., Vicary, J. A., Hörber, J. K. H., Picco, L. M., Miles, M. J., and Antognozzi, M., 2012, "Methods for imaging DNA in liquid with lateral molecular-force microscopy," Nanotechnology, vol. 23, no. 8, p. 085703.

Hoh, J. H., & Hansma, P. K. (1992). Atomic force microscopy for high-resolution imaging in cell biology. Trends in Cell Biology, 2(7), 208-213.

Howland, R. and Benatar, L., 1993, "Practical Guide to Scanning Probe Microscopy". Park Scientific Instruments: Sunnyvale, CA, USA.

James, P. J., Antognozzi, M., Tamayo, J., McMaster, T. J., Newton, J. M., and Miles, M. J., 2001, "Interpretation of contrast in tapping mode AFM and shear force microscopy. a study of Nafion," Langmuir, vol. 17, no. 2, pp. 349–360.

Leang K. K. & Fleming A. J. (2008). High-Speed Serial-Kinematic AFM Scanner - Design and Drive Considerations. American Control Conference, Westin Seattle Hotel, Seattle, Washington, USA.

Lekka, M., & Laidler, P. (2009). Applicability of AFM in cancer detection. Nature nanotechnology, 4(2), 72-72.

Physik Instrumente. (2015a). Accessed 16 Dec 2015, from website: http://www.physikinstrumente.com/product-detail-page/p-7332-p-7333-201200.html.

Physik Instrumente. (2015b). Accessed 16 Dec 2015, from website: http://www.physikinstrumente.com/product-detail-page/p-915khds-201680.html

Physik Instrumente. (2015c). Accessed 9 Feb 2015, from website: http://www.physikinstrumente.com/product-detail-page/p-882-p-888-100810.html

Polit S. & Dong J. (2009). Design of high-bandwidth high-precision flexure-based nanopositioning modules. Journal of Manufacturing Systems, 28, 71-77.

Schitter G., Astrom K.J., Dematini B., Fantner G.E. Turner K. Thurner P.J. & Hansma P.K., 2006, Design and Modeling of a High-speed Scanner for Atomic Force Microscopy. 2006 American Control Conference.

Xu, X., Melcher, J., and Raman, A., 2010, "Accurate force spectroscopy in tapping mode atomic force microscopy in liquids," Phys. Rev. B, vol. 81, pp. 035 407–1–035 407–7.

Yao, Q., Dong, J. & Ferreira, P.M.,2007. Design, analysis, fabrication and testing of a parallel-kinematic micropositioning XY stage. Intern. journal of Machine Tools & Manufacture, 47, 946-961.

Yong Y.K., Aphale S. S. & Moheimani S. O. R. (2009). Design, Identification, and Control of a Flexure-Based XY Stage for Fast Nanoscale Positioning, IEEE TRANSACTIONS ON NANOTECHNOLOGY, 8, 1.

---

[1] Note that the for the square wave demand the RMS error is not a suitable indicator: Before settling of the closed loop control, the control error for the open-loop strategy is small, while the piezo drift of the open-loop strategy causes significant steady state errors. This leads to a RMS error of 16.9nm for the closed-loop strategy, while the RMS error for the open-loop strategy is at 8nm for the square-wave demand case. Again, this is a misleading indicator of the robustness and accuracy of the closed-loop strategy. However, it shows the advantage of feedforward components.